

Flutter Analysis Based on Component Modal Synthesis for an Aeroelastic System with Structural Nonlinearities

Xiangyu Wang¹, Zhigang Wu² and Chao Yang³

School of Aeronautic Science and Engineering, Beihang University, Beijing, 100191, China

Structural nonlinearities on an aeroelastic system can significantly take influence in the dynamic responses and cause complex phenomena like the limit-cycle oscillations (LCOs). Flutter analysis for the nonlinear system thus needs special consideration for nonlinearities. In this paper, a wing-aileron system with freeplay nonlinearity and its finite-element model were constructed. Numerical investigations based on component modal synthesis (CMS) and harmonic balance (HB) method were implemented for the nonlinear flutter analysis. A wind tunnel experiment was carried out to validate the numerical results. The results derived by HB method agreed with experimental data on the linear flutter condition, LCO onset airspeed and LCO dominant frequency. The numerical diagram of LCO amplitude increasing with airspeed was also validated by experimental data. However, the experiments found that when the oscillation amplitude of wing tip was beyond the safety tolerance, the LCO of aileron was still stable and held an acceptable amplitude both numerically and experimentally, so as for determination of accurate nonlinear flutter boundary, LCOs on all of the degree of freedoms (DOFs) should be considered. The DOFs with nonlinearities were not necessarily the most dangerous one among the nonlinear system.

Nomenclature

\mathbf{u}	= structural nodal displacement vector.
\mathbf{v}	= relative displacement in the nonlinear assembly degrees of freedom (dof)
Φ	= structural modal displacement matrix.
\mathbf{q}	= general coordinates with respect to Φ .
Ψ	= inertia-relief attached modes derived by component synthesis procedure.
\mathbf{f}_J	= internal force vector, which also represents the general coordinates with respect to Ψ .
\mathbf{f}_{NL}	= nonlinear function with respect to \mathbf{v} .
\mathbf{H}	= complementary modal displacement matrix $\mathbf{H} = [\Phi \ \Psi]$.
\mathbf{M}, \mathbf{K}	= structural nodal mass and stiffness for each component (or substructures).
$\bar{\mathbf{M}}, \bar{\mathbf{C}}, \bar{\mathbf{K}}$	= general modal mass, damping and stiffness matrix for an assembled system.
$\mathbf{Q}_{qq}, \bar{\mathbf{Q}}$	= general modal force matrix for a component and for an assembled system.
ρ	= flow density (kg/m ³).
V	= flow velocity, i.e. airspeed (m/s).
d	= size of freeplay (rad).

¹ Ph.D Candidate, School of Aeronautic Science and Engineering, Beihang University, Wangxyflying@163.com.

² Associate Professor, School of Aeronautic Science and Engineering, Beihang University, wuzhigang@buaa.edu.cn

³ Professor, School of Aeronautic Science and Engineering, Beihang University, yangchao@buaa.edu.cn, and AIAA Member.

- k_0, k_e = underlying linear aileron rotational stiffness and effective stiffness (N·m/rad).
 g = artificial damping used in p-k algorithm for flutter.
 $\theta, \bar{\theta}$ = aileron rotation angle (rad), and nominal aileron rotation angle $\bar{\theta} = \theta/d$.
 U_θ, \bar{U}_θ = amplitude of θ , and amplitude of $\bar{\theta}$, i.e. $\bar{U}_\theta = U_\theta/d$.
 ω = harmonic frequency in the harmonic balance method (Hz).

Subscripts

- W = structural component label, i.e. "wing"
 A = structural component label, i.e. "aileron"
 r = rigid structural modes
 e = elastic structural modes determined by finite-element method
 h = high-order elastic modes neglected for efficiency
 J = structural grids that connect two structural components
 L = subset of J representing a linear connection
 NL = subset of J representing a nonlinear connection

I. Introduction

Flutter and limit-cycle oscillations (LCOs) are similar to some extent as both of them result from the interaction of structural dynamics, unsteady aerodynamic loads and inertia forces, but they are essentially different. Flutter is a dynamic instability phenomenon when a linear system exhibits harmonic oscillations, while LCOs can be either stable or unstable, occurs at pre- or postflutter condition, and yield amplitude-bounded and periodic motion [1]. LCOs can result in complex phenomena [2-4], affect the performance of the aircraft and even cause severe problems.

Freeplay is a typical and significant source of structural nonlinearity. The research on nonlinear flutter analysis and, in particular, on control-surface freeplay is motivated by significant number of literatures. Control-surface freeplay can be essentially classified into two types. The first functions independently, such as all-moving control surfaces or canards, in which freeplay exists in the pitching motion of the root of control surface. The other attaches to a wing and the freeplay usually exists in the rotational motion of the control surfaces.

As for the later type of control surface, take a wing-aileron system for an example, many researches have found complex LCO phenomena. Kholodar [5] calculated the flight envelopes, and found three stable LCOs with distinct frequencies occurred within the flutter onset condition. Carrese et al. [6] studied a wing with a leading-edge flap and a trailing-edge aileron. Roizner and Karpel [1] examined an aircraft with freeplay in an elevator attached to a horizontal tail, and the results presented only one LCO with a supercritical Hopf bifurcation, whose amplitude increased from zero and the dominant frequency increased continuously.

Flutter analysis determines the airspeed region in which an aircraft can keep dynamic stability and fly with safety. Many mature algorithms like p-k method [7, 8] provide a efficient path to the linear flutter analysis in the frequency domain. However, when structural nonlinearities bring LCOs to the aircraft, linear flutter analysis for an aeroelastic system can be inaccurate compared to the experiment. The accurate calculation of LCO can be very time-consuming, especially considered high-order elastic modal of component [9], preload of control system [10] and the variation of underlying linear stiffness of the freeplay actuator[11]. Component modal synthesis provide another way to address the nonlinear flutter analysis. In this paper, a wing-aileron model is constructed both numerically and physically. This aeroelastic system is divided into two linear components, the wing and the aileron, and assembled together with a nonlinear stiffness element. Numerical investigation by first-order harmonic balance approach is implemented and a wind tunnel test is carried out. The comparison between numerical results and experimental results uncovered the interesting phenomena of flutter and LCOs in nonlinear system, and validate the effectiveness of the nonlinear flutter analyzing procedure in this paper.

This paper is organized as follows. Section II.A introduces the wing-aileron model and the nonlinear actuator. Sections II.B and II.C present the structural and aerodynamic modeling methods based on component synthesis.

Section II.D introduces the procedure of nonlinear flutter analysis. Section III derives the numerical results which is compared with the experimental results.

II. Aeroelastic Model and Numerical Methods

A. Experimental and Analytical Models

An rectangular wing with an outboard trailing-edge aileron was designed and produced (see Fig. 1). It has a span of 1.40 m and the length of the wing section is 0.40 m. Seven ribs are distributed evenly along the aluminous spar of the wing. The root of the wing is oriented along the direction of flow (x-axis), and the ribs are perpendicular to the spars. The mass distribution of the wing-aileron is listed in the Table 1.

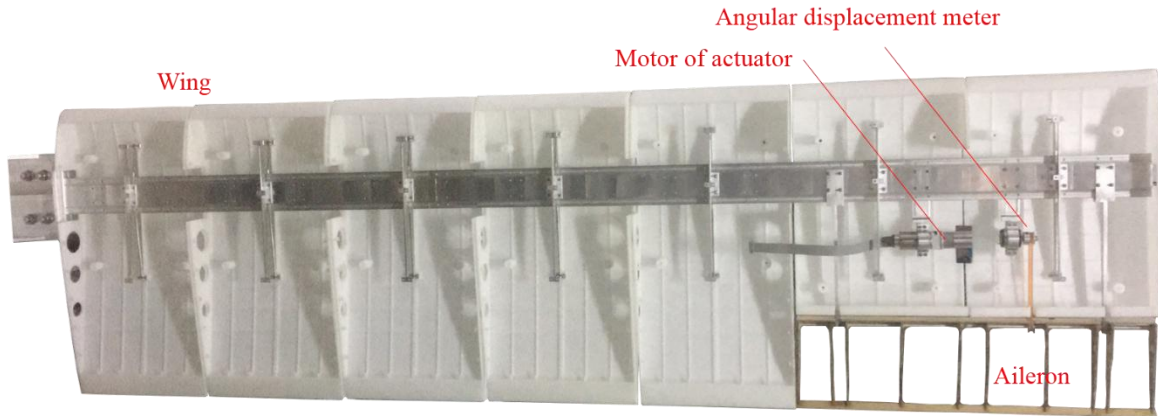


Fig. 1 Experimental model: a wing-aileron aeroelastic system

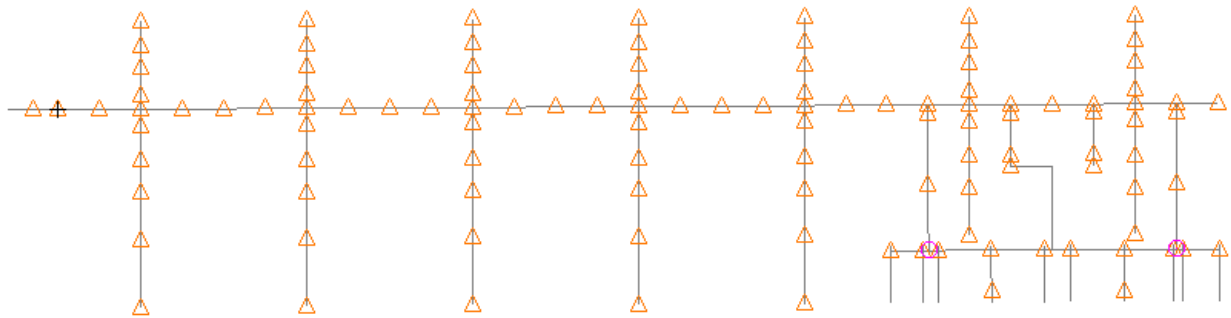


Fig. 2 Finit element model of the experimental model

Table 1 Mass distribution of the wing-aileron model

Component	Mass, g	Component	Mass, g
Wing spar	1810	Wing bars and skin	3049
Aileron	140	Aileron supporting beams	54
Acuator and supporting parts	156	Angle Meter and supporting parts	43

The aileron is mounted by two linear hinges and a nonlinear actuator that can generate freeplay. The nonlinear actuator is consist of a connector with a stop block, a rocker with a slot, and some other parts (see Fig. 3). Three rockers with different size of slots are produced, which can provided three different and reliable size of freeplay: 1.13 °, 2.50 ° and 4.00 °. Additionally, a linear actuator that combined the rocker and connector into one part is also produced to provided a linear cases. In totle, four cases labled D0, D1, D2 and D4 represent the case without freeplay and with 1.13 °, 2.50 ° and 4.00 ° degree. In the wind tunnel experiments, four cases were carried out as the sequence of D0 - D4 - D2 - D1. The angular meter was fell of and damaged in the last one, the case "D1". There were also some acceleration meters could be used for all of the cases, however, only signal captured by angular meter is used to compare with numerical results, so we apologized that only three cases, D0, D2 and D4, were adopted in this paper.

There is also an aileron rotating leaf spring produced by aluminum in the linear or nonlinear actuator. the sectional size of the leaf spring is 2.0 mm by 2.0 mm. The leaf spring provides a specific rotating stiffness of the aileron.

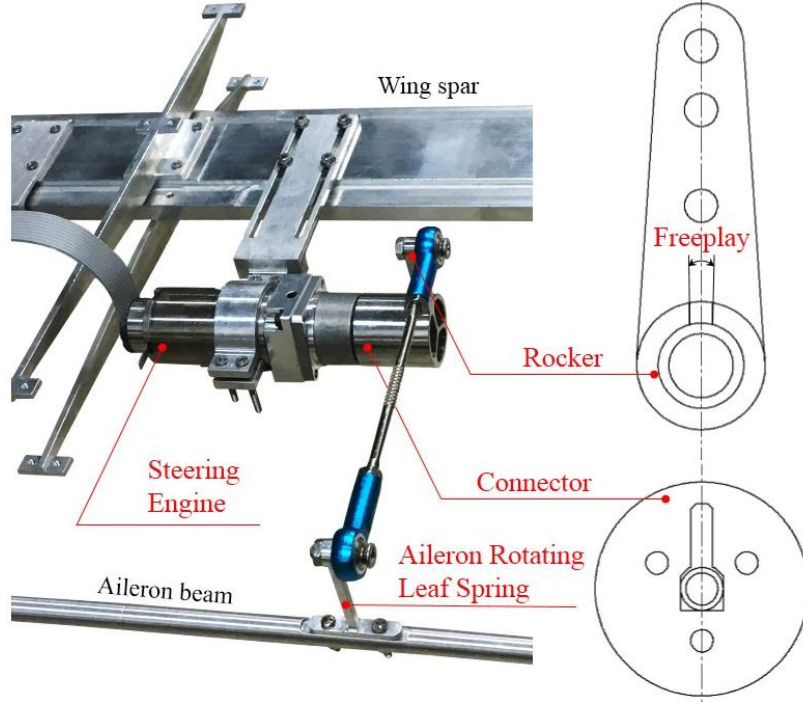


Fig. 3 Nonlinear actuator that generate specific size of rotating freeplay

B. Nonlinear Aeroelastic Modelling Based on the Component Modal Synthesis

Because concentrated structural nonlinearities usually arise in a few grids in the FEM, one approach for structural modeling is to employ the standard finite-element method to each linear component and add the minimal orders to account for the effect of the nonlinearities [12-14]. The nodal displacement vectors \mathbf{u} can be derived by the summation of the normal modes:

$$\begin{cases} \mathbf{u}_W = \Phi_{rW} \mathbf{q}_{rW} + \Phi_{eW} \mathbf{q}_{eW} + \Phi_{hW} \mathbf{q}_{hW} \\ \mathbf{u}_A = \Phi_{rA} \mathbf{q}_{rA} + \Phi_{eA} \mathbf{q}_{eA} + \Phi_{hA} \mathbf{q}_{hA} \end{cases} \quad (1)$$

where Φ and \mathbf{q} represent the modal displacement matrices and general coordinates, respectively. The subscripts r, e and h denote rigid modes, low-order elastic modes, and high-order elastic modes that are neglected for efficiency reasons. Subscripts W and A represent the wing and aileron components, respectively. As the wing is clamped at the root, Φ_{rW} is a zero matrix.

A freeplay nonlinearity in the rotation motion of the aileron can be identified as a nonlinear function between the restoring torque and deflection of the aileron, as shown in Fig. 4. The attachment modes Ψ for each component are derived by Eq. (3).

$$\Phi_h \mathbf{q}_h \approx \Psi \mathbf{f}_J \quad (2)$$

$$\Psi = \left(\Gamma^T (\bar{\mathbf{K}})^{-1} \Gamma - \Phi_e (\Phi_e^T \mathbf{K} \Phi_e)^{-1} \Phi_e^T \right) \bar{\mathbf{F}} \quad (3)$$

where \mathbf{f}_J is the internal force vector. $\bar{\mathbf{K}}$ is the subset of the nodal stiffness matrix \mathbf{K} determined by eliminating the DOFs in which the displacements are set to zero due to the constraint conditions (for a component without rigid modes) or the selection of the inertial reference frame (for a component with rigid modes). $\bar{\mathbf{F}}$ is the unit internal force matrix, and Γ is the inertial-balanced matrix:

$$\Gamma = \begin{cases} \mathbf{I} - \mathbf{M}\Phi_r\Phi_r^T & , \Phi_r \neq \mathbf{0} \\ \mathbf{I} & , \Phi_r = \mathbf{0} \end{cases} \quad (4)$$

The complementary modal matrix $\mathbf{H} = [\Phi_r \ \Phi_e \ \Psi]$ and the corresponding general coordinates $\mathbf{p} = [\mathbf{q}_r^T \ \mathbf{q}_k^T \ \mathbf{f}_j^T]^T$ can be defined for each component. Thus, Eq. (1) can be rewritten as follows:

$$\begin{cases} \mathbf{u}_W = \mathbf{H}_W \mathbf{p}_W \\ \mathbf{u}_A = \mathbf{H}_A \mathbf{p}_A \end{cases} \quad (5)$$

An assembly process can be implemented by the compatibility conditions for the displacements and internal forces.

$$\begin{cases} \mathbf{u}_{LW} = \mathbf{u}_{LA} \\ \mathbf{u}_{NLW} = \mathbf{u}_{NLA} + \mathbf{v} \end{cases} \quad (6)$$

$$\begin{cases} \mathbf{f}_{LW} = -\mathbf{f}_{LA} \\ \mathbf{f}_{NLW} = -\mathbf{f}_{NLA} \end{cases} \quad (7)$$

The subscripts L and NL represent the linear and nonlinear DOFs, respectively, between the wing and aileron. \mathbf{v} is a relative displacement in the nonlinear assembly DOFs. Thus, the modal reduction equation can be written as follows:

$$\mathbf{p}_{AB} = \mathbf{T} \begin{bmatrix} \mathbf{q}_c \\ \mathbf{v} \end{bmatrix} \quad (8)$$

where \mathbf{T} is the assembly matrix; \mathbf{p}_{AB} is the combination of two complementary general coordinates, namely, $[\mathbf{q}_{fW}^T \ \mathbf{q}_{kW}^T \ \mathbf{f}_{jW}^T \ \mathbf{q}_{fA}^T \ \mathbf{q}_{kA}^T \ \mathbf{f}_{jA}^T]^T$; and \mathbf{q}_c consists of the elastic modes of each component, namely, $[\mathbf{q}_{fW}^T \ \mathbf{q}_{kW}^T \ \mathbf{q}_{fA}^T \ \mathbf{q}_{kA}^T]^T$. The complete aeroelastic equation of the wing-aileron model can be derived [11] as follows:

$$\bar{\mathbf{M}}_{qq} \begin{bmatrix} \ddot{\mathbf{q}}_c \\ \ddot{\mathbf{v}} \end{bmatrix} + \bar{\mathbf{C}}_{qq} \begin{bmatrix} \dot{\mathbf{q}}_c \\ \dot{\mathbf{v}} \end{bmatrix} + \bar{\mathbf{K}}_{qq} \begin{bmatrix} \mathbf{q}_c \\ \mathbf{v} \end{bmatrix} = \begin{bmatrix} \mathbf{0} \\ \mathbf{f}_{NL}(\mathbf{v}) \end{bmatrix} + \frac{1}{2} \rho V^2 \bar{\mathbf{Q}}_{qq} \begin{bmatrix} \mathbf{q}_c \\ \mathbf{v} \end{bmatrix} \quad (9)$$

where $\bar{\mathbf{M}}_{qq}$, $\bar{\mathbf{C}}_{qq}$ and $\bar{\mathbf{K}}_{qq}$ are the modal mass, damping, and stiffness matrices of the wing-aileron model, respectively. $\mathbf{f}_{NL}(\mathbf{v})$ is the nonlinear force vector. ρ and V are the flow density and velocity, respectively. $\bar{\mathbf{Q}}_{qq}$ is the modal aerodynamic force matrix. In the wing-aileron model proposed in this paper, \mathbf{v} denotes the rotation angle of the aileron θ , and $\mathbf{f}_{NL}(\mathbf{v})$ represents the freeplay restoring torque of the aileron $T_A(\theta)$:

$$T_A(\theta) = \begin{cases} k_0(\theta - d) & \theta > d \\ 0 & -d \leq \theta \leq d \\ k_0(\theta + d) & \theta < -d \end{cases} \quad (10)$$

where d is the degree of freeplay, and k_0 is the underlying linear stiffness, which must be validated by a ground vibration test (GVT). The freeplay nonlinearity is depicted in Fig. 4.

C. Aerodynamic Modelling

An unsteady doublet-lattice method is employed to model the flow about the wing-aileron model. The aerodynamic lattices include a 19×7 grid for the inside wing and a 7×5 grid for the outside wing. The aileron occupies a 7×2 grid located outboard of the wing and aft along the chordwise direction.

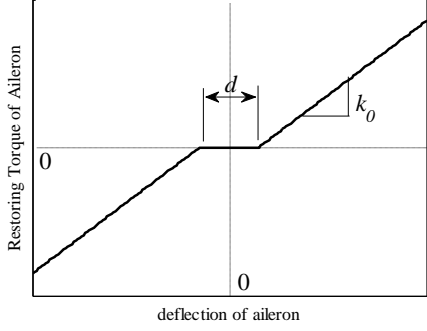


Fig. 4 The freeplay function

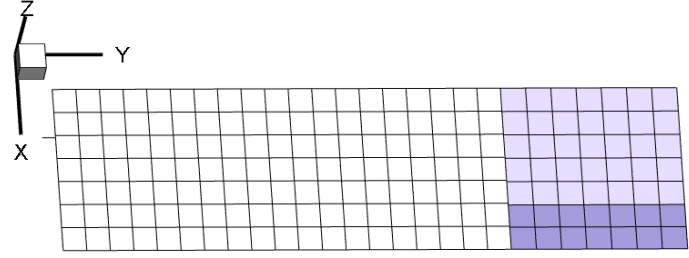


Fig. 5 Aerodynamic grids of the wing-aileron model

The modal aerodynamic force matrix has the following formulation [11]:

$$\bar{\mathbf{Q}}_{qq} = \mathbf{T}^T \cdot \begin{bmatrix} \bar{\mathbf{H}}_W^T & \\ & \bar{\mathbf{H}}_A^T \end{bmatrix} \cdot \bar{\mathbf{Q}}_{gq}(k) \quad (11)$$

where k is the reduced frequency, and $\bar{\mathbf{Q}}_{gq}$ reflects the forces on each structural grid with respect to the extended complementary modal motion: $[\bar{\mathbf{H}}_W \ \bar{\mathbf{H}}_A]$. $\bar{\mathbf{H}}_W$ adds the nodes of the aileron to \mathbf{H}_W , and $\bar{\mathbf{H}}_A$ adds the nodes of the wing to \mathbf{H}_A . Finally, the complete aeroelastic equation can be written as follows:

$$\bar{\mathbf{M}}_{qq} \begin{bmatrix} \ddot{\mathbf{q}}_c \\ \ddot{\theta} \end{bmatrix} + \bar{\mathbf{C}}_{qq} \begin{bmatrix} \dot{\mathbf{q}}_c \\ \dot{\theta} \end{bmatrix} + \bar{\mathbf{K}}_{qq} \begin{bmatrix} \mathbf{q}_c \\ \theta \end{bmatrix} = \begin{bmatrix} \mathbf{0} \\ T_A(\theta) \end{bmatrix} + \frac{1}{2} \rho V^2 \bar{\mathbf{Q}}_{qq}(k) \begin{bmatrix} \mathbf{q}_c \\ \theta \end{bmatrix} \quad (12)$$

D. Harmonic Balance Method and Flutter Analysis in Frequency domain

as Eq. (12) describes the freeplay using an explicit expression, the standard HB method can be utilized in a straightforward manner. The first-order HB (1-HB) method, also known as the describing function approach, constructs a nonlinear effective stiffness k_{eff} (see Table 2 in Ref. [15]):

$$k_{\text{eff}} = k_0 \left(1 - \frac{2}{\pi} \arcsin \frac{d}{U_\theta} - \frac{2}{\pi} \cdot \frac{d}{U_\theta} \sqrt{1 - \left(\frac{d}{U_\theta} \right)^2} \right) \quad (13)$$

where d is the degree of freeplay, and U_θ is the amplitude of the aileron rotation angle. Then, the amplitude of the aileron restoring torque can be expressed as follows:

$$U_T = k_{\text{eff}} \cdot U_\theta \quad (14)$$

Accordingly, Eq. (12) can be analyzed using the following equation, which is also known as the K method flutter equation:

$$\left(-\omega^2 \bar{\mathbf{M}}_{qq} + i\omega \bar{\mathbf{C}}_{qq} + (1+ig) \bar{\mathbf{K}}_{qq} - \begin{bmatrix} \mathbf{0} & \mathbf{0} \\ \mathbf{0} & k_{\text{eff}}(\bar{U}_\theta) \end{bmatrix} - \frac{1}{2} \rho V^2 \bar{\mathbf{Q}}_{qq}(k) \right) \begin{bmatrix} \mathbf{U}_c \\ U_\theta \end{bmatrix} = \begin{bmatrix} \mathbf{0} \\ 0 \end{bmatrix} \quad (15)$$

where i is the unit imaginary number; g is the artificial damping; \bar{U}_θ is the nominal amplitude of the aileron rotational angle, $\bar{U}_\theta = U_\theta/d$; and \mathbf{U}_c is the amplitude of \mathbf{q}_c .

III. Numerical Results and Experimental Validation

A. Underlying Linear Stiffness Determination and Linear flutter analysis.

A series of ground vibration tests (GVTs) were implemented to the linear system "D0", so that the stiffness of the leaf spring (see Fig. 4) was determined to be 2.9 N.m/rad. Then a structural dynamic analysis based on the method mentioned in the Section II was carried out, and the results were compared with linear analysis using MSC. NASTRAN. In the CMS algorithm, the first 5 orders of the wing and the first 6 orders of the aileron are used, together

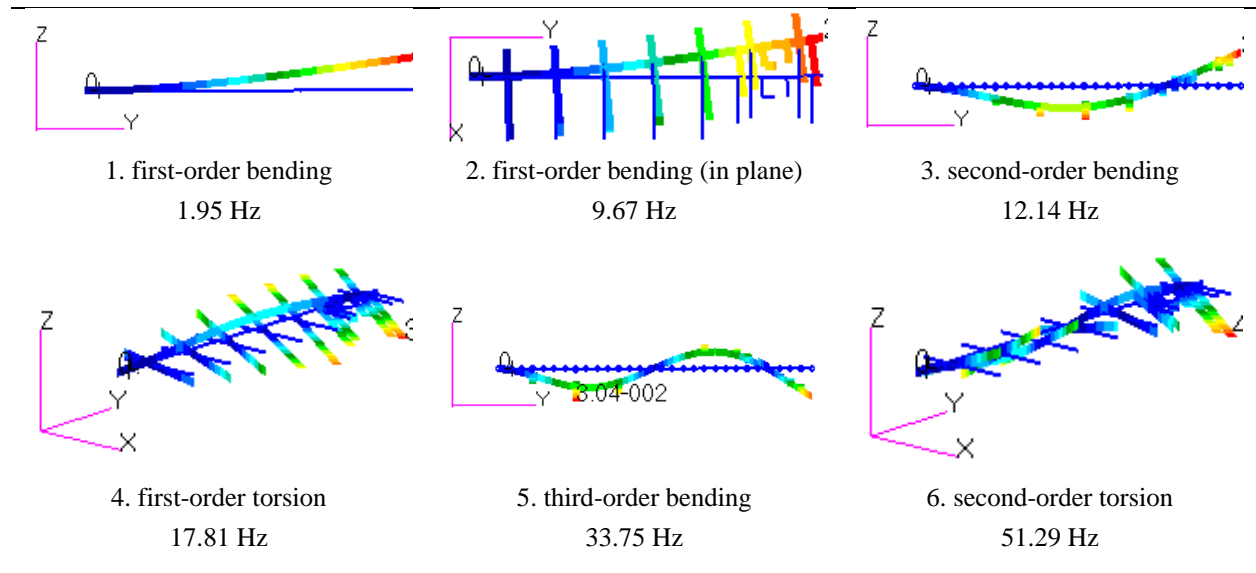
with one nonlinear dof (rotational angle of the aileron), the final order of the assembled system is $12 = 5+6+1$. Table 1 lists the first 5 modal frequencies of the assembled system.

A linear flutter analysis for the assembled system was then carried out. The results showed that the linear flutter of the system is 49.92 m/s, and the flutter frequency is 13.89 Hz.

Table 2 Structural analysis of the numerical model

FEM for linear wing-aileron model, Hz	FEM for component of the wing (clamped at root), Hz	FEM for component of the aileron (free-free bounded), Hz	FEM for assembled wing-aileron model using CMS method, Hz
1.89	1.95	first six rigid modes: 0.00	1.89
9.36	9.67	78.54	9.34
12.07	12.14	...	12.07
12.71	17.81		12.71
19.73	33.75		19.73

Table 3 Structural modal analysis for wing component



B. Nonlinear flutter analysis and experimental validation

In this section, the nonlinear aeroelastic equation is solved in the frequency domain via the method mentioned in the Section I. The modal damping matrix is set to zero matrix. The atmospheric density is 1.225 kg/m^3 , and the reference length is 0.40 m.

In Fig. 6 and Fig. 7, the numerical results (label CMS+HB1) of the oscillation of aileron rotational motion uncover a harmonic oscillation that occurs at the airspeed of 32.14 m/s with the frequency of 15.5 Hz. Since the amplitude of this oscillation varies only within a very limited region as the airspeed increased, it can be considered as a sign of stable LCO. When the airspeed keep increasing, the amplitude frequency of LCO increases slowly at first, and booms dramatically when the airspeed is over around 47.0 m/s, and the frequency increases alightly at first, and then drop quickly until the linear flutter frequency 13.89 Hz.

Wind tunnel experiements uncover more details of this LCO. As shown in Fig. 8 and Fig. 9, when the airspeed hold on 33.0 m/s, only one dominant frequency around 15.0 Hz is found, and the phase diagram of aileron rotational angle consists of numerous random points. When the airspeed increased to 33.5 m/s, however, three dominant frequencies occurs (around 15.0 Hz, 30.0 Hz, and 45.0 Hz) and the diagram present a circle, which indicate that the

signal captured in angular meter is periodical. As the airspeed continue increasing to 35.3 m/s, the three dominant frequencies and the shape of the circle in phase diagram are almost unchangless.

The weighted average of the three dominant frequencies is about 1 Hz higher than the numerical results (Fig. 7) since HB method cannot account for the high order harmonics. The diagram of oscillation amplitude vs airspeed from experimental data present a good validation of numerical results (Fig. 6). The experimental data in Fig. 6 and Fig. 7 stopped at airspeed of 35.3 m/s for 4.0° freeplay and 33.8 m/s for 2.5° freeplay, because the amplitude of wing tip motion was so large that we had to stop the wind tunnel for the safety of the model. The aileron LCO were still stable at that two experimental data point.

Table 4 present the value of flutter or LCO onset airspeed and average dominant frequency, on which experimental data basically agree with the numerical results.

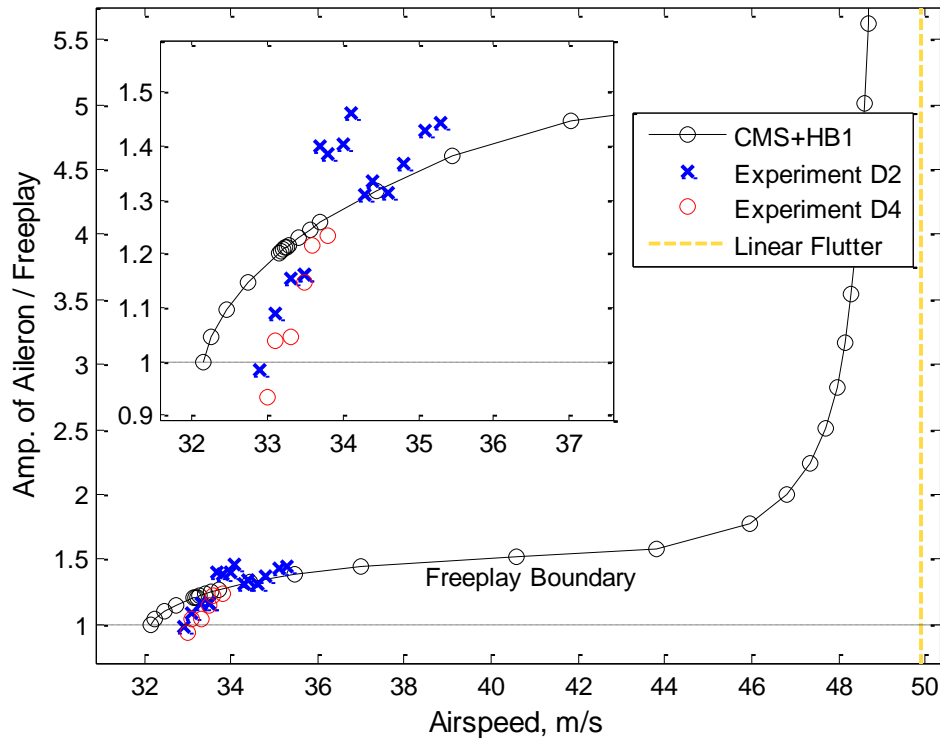


Fig. 6 Nonlinear flutter results: airspeed vs relative amplitude of aileron

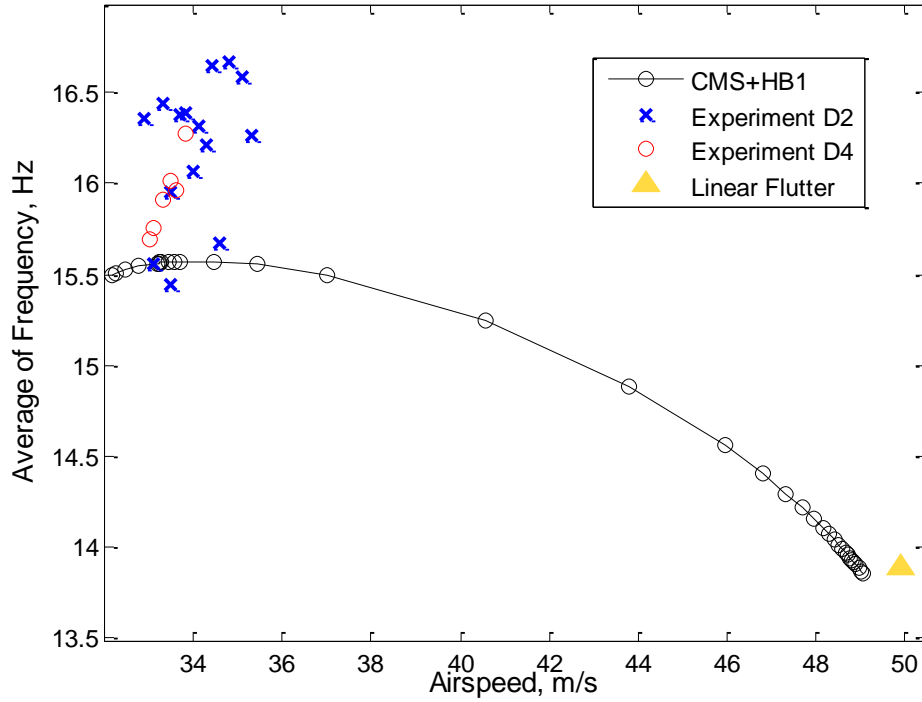


Fig. 7 Nonlinear flutter results (V- ω plot)

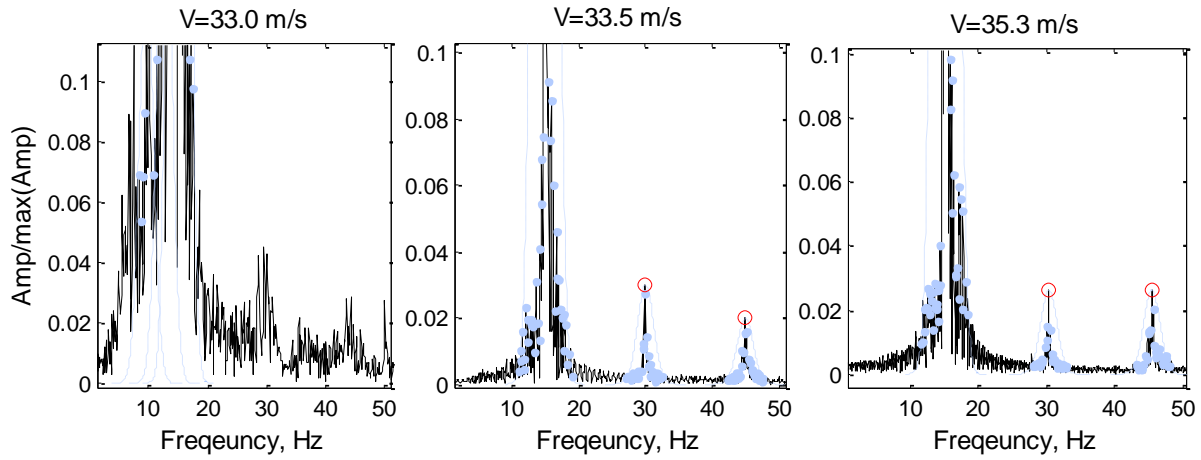


Fig. 8 FFT of aileron rotating signal from wind tunnel data, 2.5° freeplay

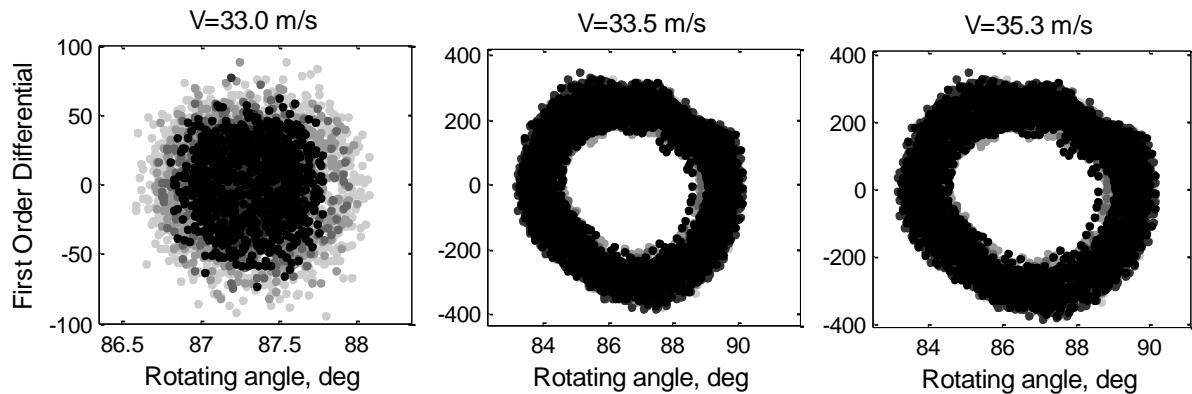


Fig. 9 phase diagram of aileron rotation angle from wind tunnel data, 2.5 ° freeplay**Table 4 Numerical results vs experimental data for the nonlinear flutter and LCOs**

size of freeplay	oscillation onset airspeed, m/s		oscillation type		average harmonic frequency of the oscillation at its onset airspeed (Hz)	
	numerical	test	numerical	test	numerical	test
Linear	49.92	> 45.5 m/s	flutter	flutter	13.89	13.55
2.50°	32.14	33.5 m/s	LCO	LCO	15.50	15.44
4.00°	32.14	33.0 m/s	LCO	LCO	15.50	15.69

Acknowledgments

This research is supported by the Civil Aircraft Safety Foundation of China (No. AADSA2016022) and the foundation of NSFC 11372023. The authors thank the Shanghai Aircraft Airworthiness Certification Center for many technical discussions.

Conclusion

- 1) This paper presents the aeroelastic modelling procedure for a wing-aileron system with a freeplay on aileron rotational motion. The modelling method is based on component modal synthesis and has the following advantages:
 - a) This method can be utilized in an aeroelastic system with any number of structural nonlinearities, and the nonlinearities can be expressed explicitly in the aeroelastic equation.
 - b) Unsteady aerodynamic loads are derived only by linear components' rigid modes, some low-order elastic modes and inertia-relief attached modes, which are independent of structural nonlinearities. As a result, classic codes for flutter analysis (e.g. p-k method) can be implemented without re-calculating aerodynamic loads when the effective stiffness of the structural nonlinearities change, and nonlinear flutter analysis based on the HB method can be carried out with efficiency.
- 2) Numerical results uncover the basic characteristics of LCO and agree with the experimental results.
 - a) For a linear system, flutter occurs at the airspeed over 45.5 m/s (experimentally), or more specifically, at around 50.0 m/s (numerically). The flutter frequency derived by experiment and calculation are 13.55 Hz and 13.89 Hz, respectively.
 - b) Both the numerical results and experimental data show that LCO occurs at 32.0 m/s ~ 33.5 m/s, and the dominant frequency of LCO is around 15.5 Hz.
 - c) The plot of LCO amplitude increasing with airspeed derived by numerical results agrees with the experimental data when the airspeed is lower than 36.0 m/s. After this airspeed, the experimental data in Fig. 6 and Fig. 7 stopped because the amplitude of wing tip motion was so large that we had to stop the wind tunnel for the safety of the model. The aileron LCO was still stable at those two experimental data points. So, if we want to use this procedure to determine the nonlinear flutter boundary, the amplitude of LCO for the wing tip point should be considered as well, rather than only considering the aileron rotational motion.

References

- [1] Roizner, F., and Karpel, M., "Parametric flutter margin method for aeroservoelastic stability analysis," *AIAA Journal*, Vol. 56, No. 3, 2018, pp. 1011-1022.
doi:10.2514/1.J056514
- [2] Hodges, D. H., and Pierce, G. A., *Introduction to structural dynamics and aeroelasticity*. 2nd ed., Cambridge University Press, 2011.
- [3] Dimitriadis, G., "Complete Bifurcation Behaviour of Aeroelastic Systems with Freeplay," *52nd AIAA/ASCE/ASC Structures, Structural Dynamics, and Materials Conference*, Denver, Colorado, 2011.
doi:10.2514/6.2011-2142
- [4] Dowell, E. H., "Some recent advances in nonlinear aeroelasticity: Fluid-structure interaction in the 21st century," *AIAA/ASME/ASCE/AHS/ASC Structures, Structural Dynamics, and Materials Conference*, Orlando, Florida, 2010.
doi:10.2514/6.2010-3137
- [5] Kholodar, D. B., "Aircraft control surface and store freeplay-induced vibrations in aeroelastic stability envelope," *Journal of Aircraft*, Vol. 53, No. 5, 2016, pp. 1538-1549.
doi:10.2514/1.C033772

- [6] Carrese, R., Joseph, N., Marzocca, P., and Levinski, O., "Aeroelastic response of the AGARD445.6 wing with freeplay nonlinearity," *58th AIAA/ASCE/AHS/ASC Structures, Structural Dynamics, and Materials Conference*, Grapevine, Texas, 2017.
doi:10.2514/6.2017-0416
- [7] Irwin, C. A., and Gueyet, P. R., *The Subcritical Response and Flutter of a Swept Wing Model*, Royal Aircraft Establishment, 1965.
- [8] Hassig, H. J., "An Approximate True Damping Solution of the Flutter Equation by Determinant Iteration," *Journal of Aircraft*, Vol. 8, No. 11, 1971, pp. 885-889.
- [9] Park, Y., Yoo, J., and Lee, I., "Nonlinear aeroelastic analysis of control with freeplay in transonic region," *AIAA Journal*, Vol. 45, No. 5, 2007, pp. 1142-1146.
doi:10.2514/1.14068
- [10] Yang, N., Wu, Z., and Yang, C., "Structural nonlinear flutter characteristics analysis for an actuator-fin system with dynamic stiffness," *Chinese Journal of Aeronautics*, Vol. 24, 2011, pp. 590-599.
doi:10.1016/S1000-9361(11)60069-1
- [11] Wang, X., Wu, Z., Yang, C., and He, X., "Substructure-based flutter analysis for a wing-aileron system with freeplay," *2018 AIAA/ASCE/AHS/ASC Structures, Structural Dynamics, and Materials Conference*, Kissimmee, Florida, 2018.
doi:10.2514/6.2018-0953
- [12] Carig, R. R., and Bampton, M. C. C., "Coupling of Substructures for Dynamic Analyses," *AIAA Journal*, Vol. 6, No. 7, 1968, pp. 1313-1319.
doi: 10.2514/3.4741
- [13] Rubin, S., "Improved Component-Mode Representation for Structural Dynamic Analysis," *AIAA Journal*, Vol. 13, No. 8, 1975, pp. 995-1006.
doi:10.2514/3.60497
- [14] Hintz, R. M., "Analytical Methods in Component Modal Synthesis," *AIAA Journal*, Vol. 13, No. 8, 1975, pp. 1007-1016.
doi:10.2514/3.60498
- [15] Padmanabhan, M. A., Dowell, E. H., and Pasilio, C. L., "Computational study of aeroelastic limit cycles due to localized structural nonlinearities," *Journal of Aircraft*, 2018, pp. 1-11.
doi:10.2514/1.C034645